New sol-gel-derived magnetic bioactive glass-ceramics containing superparamagnetic hematite nanocrystals for hyperthermia application

New sol-gel-derived magnetic bioactive glass-ceramics containing superparamagnetic hematite nanocrystals for hyperthermia application

Roger Borges[1], Leticie M. Ferreira[1], Carlos Rettori[1, 2], Isis O. dos Santos[1], Francesco Baino[3], Juliana Marchi[1]

1. Centro de Ciências Naturais e Humanas, Universidade Federal do ABC, Santo André, SP, Brazil
2. Instituto de Física Gleb Wataghin, Universidade Estadual de Campinas, Campinas, SP, Brazil
3. Department of Applied Science and Technology, Politecnico di Torino, Turin, Italy

Abstract

Although the three main phases of iron oxide – hematite, maghemite and magnetite – exhibit superparamagnetic properties at the nanoscale, only maghemite and magnetite phases has been explored in magnetic bioactive glass-ceramics aimed to applications in cancer treatment by hyperthermia. In this work, we report for first time the superparamagnetic properties of hematite nanocrystals grown in a 58S bioactive glass matrix obtained by a sol-gel method. The glass-ceramics were based on the (100-x)(58SiO_2-33CaO-9P_2O_5)-xFe_2O_3 system (x = 10, 20 and 30 wt.%), and were characterized by X-ray diffraction, dynamic light scattering and VSM-SQUID magnetometer. Their ability to produce heat under an alternating magnetic field was investigated by calorimetric test. Furthermore, the bioactivity of the glass-ceramics was analyzed in simulated body fluid (SBF) solution, and the cytotoxicity was studied with MC3T3-E1 pre-osteoblast cells. The thermal treatment led to the growth of hematite (α-Fe_2O_3) nanocrystals, conferring superparamagnetic properties to the glass-ceramics, which was enough to produce heat under an external alternating magnetic field. Besides, the crystallization did not inhibit materials bioactivity, evidenced by the formation of calcium phosphate onto the glass-ceramic surface upon soaking in SBF. Besides, their cytotoxicity was similar to other magnetic bioactive glass-ceramics reported in the literature. Finally, these results suggested that the superparamagnetic properties of hematite nanocrystals can be explored in multifunctional glass-ceramics applied in bone cancer treatment by hyperthermia allied to bone regeneration.

Keywords: Bioactive Glasses, Glass-Ceramic, Superparamagnetism, Hyperthermia, Sol-Gel

1. INTRODUCTION

Iron oxides are among the most commonly used materials for biomedical applications, especially for magnetic hyperthermia due to their magnetic properties, low cost, and low cytotoxicity. These oxides can be found as different compounds in nature, such as hematite (α-Fe_2O_3), magnetite (Fe_3O_4) and maghemite (γ-Fe_2O_3) (1). Magnetite and maghemite are intrinsic ferrimagnetic materials since their net spins are not entirely compensated, resulting in a non-zero net magnetic moment.

On the contrary, the magnetic properties of hematite arise from thermally-induced changes in the crystal structure. Hematite has a rhombohedral lattice and hexagonal cell unit with parameters a = 0.5034 nm and c = 1.375 nm. Hematite has its iron ion spins antiparallelly ordered at a temperature below Neel Temperature (≈955 K). Furthermore, when hematite particle is in the micrometric scale, it has a thermal transition at ≈263 K, i.e. the so-called Morin Transition. Below such transition, the lattices of iron and oxygen elements are oriented with the plane axis [111] and are antiparallel, thus conferring antiferromagnetic properties. However, above Morin Transition, the magnetic moments are on the basal plane (111), but canted from the antiferromagnetic axis; it results in a weak ferrimagnetic plane, making hematite a ferrimagnetic material above such Morin Transition (2). Interestingly, the Morin Transition can be shifted towards lower temperatures when the hematite crystals change from micrometric to nanometric size. For example, particles smaller than 8-20 nm have Morin Transition below 4 K. Such a phenomenon has been associated with expansion and tension of crystal lattice in hematite nanoparticles (2).

When iron oxides, like hematite, magnetite, or maghemite phases, have particle size below 100 nm, there is an absence of multiple magnetic domains, and the whole particle behaves as a single domain with a resulting giant magnetic moment. Under those conditions, the magnetization fluctuates in orientation, and above a given temperature, these iron oxides behave like superparamagnetic materials (3). When these particles are exposed to an externally applied alternating magnetic field, they can either rotate or align their magnetization with the applied magnetic field, which are phenomena related to Brownian or Neel mechanisms, respectively. Under these situations, there will be a loss of magnetic energy, which is dissipated as heat in their surroundings, thereby causing an increase in temperature of the whole system (4). The ability to convert magnetic energy into heat is the basis of magnetic hyperthermia. In brief, (bio)materials containing these iron oxide phases at the nanoscale can be placed next to tumors and kills cancer cells by hyperthermia if an external alternating magnetic field is applied (3,5).

Bioactive glasses and glass-ceramics are biocompatible and bioactive materials, i.e., they have the ability to nucleate a bone-like apatite layer on their surface when immersed in the body fluid. By forming such an apatite layer on the surface, these glasses and glass-ceramics can establish tight chemical bonds with bone tissue, thus improving osseointegration between implant material and living tissue (6–10). Given that these glasses can be doped with several elements from the periodic table or can be crystallized without significant loss of bioactive properties, it is possible to develop glass-ceramics containing magnetic phases dispersed in the glass structure, which can also be used in magnetic hyperthermia (11). In this case, these materials can simultaneously treat the tumor and regenerate the bone defect caused by tumor

growth (12). This is possible because the magnetic phase has suitable magnetic properties for hyperthermia applications, while the bioactive glass matrix has biological properties that make them suitable for bone regeneration applications.

The first magnetic bioactive glass-ceramic was introduced in 1991, based on the SiO_2-CaO-Fe_2O_3-B_2O_3-P_2O_5 system, and it was produced by melt-quenching method followed by crystallization for the growth of magnetic phases (13,14). Since then, many other magnetic bioactive glass-ceramics were proposed in the literature and produced by crystallization of melt-derived glasses (15). It is essential to take into account that bioactivity and magnetic properties are competing properties, since the growth of magnetic and other undesired crystalline phases during thermal treatments may cause an increase in the chemical durability of these glasses, thereby slowing the rate of reaction steps involved in bioactivity process (16). The sol-gel approach may be an alternative technique to produce these glasses since glasses obtained by this method are typically more bioactive than melt-quenched ones due to their higher surface area (10,11,17).

The main disadvantage of the sol-gel method is the abrupt pH change along with the synthesis, which sometimes causes the precipitation of undesired phases depending on the raw materials used. In particular, this issue restrains the development of magnetic bioactive glasses by sol-gel method, since soluble compounds of iron (III) or iron (II) are typically used as the precursors of magnetite, and precipitate as iron oxide during the pH change of the synthesis (1). In order to overcome such restriction, different alternatives have been proposed in the literature, including a mixture of sol-gel and melt-derived magnetic glass (18–21), the growth of magnetite crystals confined in mesoporous bioactive glasses produced by evaporation-induced

self-assembly (EISA) (22,23), and the growth of maghemite crystals within the pores of bioactive glass scaffolds (24–26).

However, all these strategies still have disadvantages to be overcome, which can be summarized into two main points: I) nucleation of undesired crystalline phases that inhibit bioactivity; II) the saturation magnetization of these glasses is low, which leads to the production of magnetic materials with low efficiency in transforming magnetic energy into heat. Thus, the development of magnetic glasses by a one-pot sol-gel method is still a challenge. In this work, we propose alternative processing of bioactive glass-ceramics containing nanocrystals of hematite that behaves as a superparamagnetic material, being able to be potentially used in hyperthermia treatments.

2. MATERIALS AND METHODS

2.1 Materials

All raw materials used in this work were analytical grade reagents: tetraethyl orthosilicate (TEOS, > 98% Sigma Aldrich), triethyl phosphate (TEP, > 99% Sigma Aldrich), calcium nitrate tetrahydrate ($Ca(NO_3)_2.4H_2O$ > 98%, Sigma Aldrich), ethanol (> 98%, Sigma Aldrich), iron (III) nitrate nonahydrate ($Fe(NO_3)_3.9H_2O$ > 99%, Sigma Aldrich), iron (II) chloride tetrahydrate ($FeCl_2.4H_2O$ > 99%, Sigma Aldrich) and ultrapure water (Milli Q, USA).

2.2 Synthesis of glass-ceramic systems

The synthesis procedure used in this work was a modification of the quick alkali-mediated method proposed elsewhere (27). Briefly, TEOS and TEP were hydrolyzed for 20 min in a solution containing water, 2 M HNO_3, and ethanol. Then, 1 M ammonia solution was added in the acidic solution leading to the condensation of TEOS and TEP, till a gel consistency was achieved. The gel was freeze-dried (Operon, South Corea) for 24 h. The dried gel was suspended in water, and calcium nitrate tetrahydrate, iron (III) nitrate nonahydrate, and iron (II) chloride tetrahydrate were sequentially added in the suspension and stirred for 20 min. Iron nitrate and chloride were added in the solution in a 2:1 weight ratio, aiming to obtain glasses based on the (100-Y)(58SiO_2-33CaO-9P_2O_5)YFe_2O_3 system, where Y = 10, 20 and 30 wt.%. The final suspension was freeze-dried, followed by calcination at 550°C for 1 h (Furnace EGD 300, Brazil). Calcined materials were submitted to a thermal treatment at 670°C for 1 h (Furnace EGD 300, Brazil) in order to induce the nucleation of hematite nanocrystals. The glass-ceramics produced in this work ("GCFe-Y") are listed in Table 1.

Table 1 – Glass-ceramic compositions studied in this work, based on the 58S bioactive glass (27) with different additions of iron (III) oxide.

Nomenclature	**Composition (wt.%)**
GCFe10	90(58SiO_2-33CaO-9P_2O_5)·10Fe_2O_3
GCFe20	80(58SiO_2-33CaO-9P_2O_5)·20Fe_2O_3
GCFe30	70(58SiO_2-33CaO-9P_2O_5)·30Fe_2O_3

2.3 Characterization

2.3.1 Structural and magnetic properties

The GCFe glass-ceramics were characterized by wide-angle X-ray diffraction (XRD) in order to infer their microstructure. Analyses were carried out in a D8 Focus diffractometer (Bruker AXS, USA), between 10° and 70° 2θ and 2°/min step. The XRD results were used to estimate the crystal size of the hematite phase by using Scherrer equation (Eq. 1) (28), and also to quantify the amount of crystalline phase (Eq. 2) (29,30):

$$\tau = \frac{K\lambda}{\beta cos\theta} \text{ Eq. 1}$$

$$C = R_x \times 100 \text{ Eq. 2}$$

where τ is the mean size of the crystalline domain, K is a dimensionless shape factor assumed to be 0.9, λ is the X-ray wavelength, β is the line broadening at half the maximum intensity (FWHM), and θ is the Bragg angle. Regarding Eq. 2, C is the amount of crystalline phase, and R_x is the ratio of the area under the crystalline peaks to the total area.

The particle size distribution was determined by dynamic light scattering (DLS), where measurements were carried out in a NanoZetasizer (Malvern) equipment with an angle of 183° and 633 nm wavelength.

The superparamagnetic properties of the glass-ceramics were characterized in a VSM-SQUID through the measurement of magnetization as a function of an applied static magnetic field between -60 and 60 kOe (MxH), and magnetization as a function of temperature in a low magnetic field cooling – zero-field cooling (FC-ZFC). For the FC-ZFC curves, the samples were

cooled until 2 K without magnetic field; then, a field of 500 Oe was applied, and the temperature was increased up to 300 K (ZFC measurement); after that, the samples were cooled again under a 500 Oe applied field (FC measurement).

2.3.2 Calorimetric tests

The capability of the glass-ceramics to generate heat when exposed to an alternating magnetic field was estimated using a magnetic induction furnace (Egma 6, Felmi S.r.l, Genova, Italy) according to the experimental setup described in previous work (31) This furnace was able to generate an applied magnetic field of maximum amplitude equal to 31.2 kA/m, corresponding to 6 kW of radiofrequency power, with a fixed working frequency of 220 kHz.

In order to perform the test, the glass-ceramic powders were placed in an optically-transparent glass tube (diameter 10 mm, length 160 mm) filled with distilled water, using a mass-to-volume ratio of 20 mg/mL. A polyethylene foam was placed around the tube as a thermal insulator (λ = 0.038 W/m K) in order to reduce the heat dispersion towards the outer environment.

The increment of the water temperature was measured at fixed time points (2, 4, 6, 8, 10, and 12 min) by using a digital thermocouple (Datalogger, Tersid S.p.A. Milano, Italy). Results were reported as mean ± standard deviation over triplicate experiments.

2.3.3 Bioactivity test

The bioactivity test was employed to study the glass-ceramic ability to form hydroxyapatite on its surface after immersion in SBF (simulated body fluid) solution. SBF solution was prepared according to Kokubo & Takadama (16) method, and the experimental

procedure to perform the test was based on Maçon et al. (32). In Brief, 75 mg of each glass-ceramic powder was immersed in 50 mL of SBF solution, and maintained in an orbital shaker (Solab Model SL-222, Brazil) at 120 rpm, up to 7 days at physiological conditions (37 °C and pH 7.4).

After the test, the glass-ceramic powders were filtered and exhaustively rinsed with ultrapure water, ethanol, and finally with acetone to block further hydration reactions. Then, the powders were structurally characterized by XRD and FTIR, and their surface morphology was analyzed by SEM-EDS.

The FTIR results were used to quantify the amount of hydroxyapatite grown on the glass surface by employing a methodology described by Yu et al. (33). Briefly, glass-ceramic powders after immersion in SBF solution were mixed with iron III thiocyanate (purity > 99 %, Sigma Aldrich) and KBr (purity > 99 %, Sigma Aldrich) to prepare pellets for FTIR measurements using transmission mode (Varian-Agilent). Another pellet containing synthetic hydroxyapatite (purity > 97 %, Sigma Aldrich) was prepared by replacing the amount of glass-ceramic powder, and it was employed as a standard sample. For both pellets, iron III thiocyanate was used as an internal standard to normalize the spectra at the C≡N bond (2121 cm^{-1}). Then, the area under the curve corresponding to the $P=O_{crystalline}$ bond (560-605 cm^{-1}) was determined (A_{SBF}) and compared with the area of the standard sample (A_{HA}). The amount of hydroxyapatite in each sample was determined using the Eq. 3.

$$(A_{SBF} \times 100) / A_{HA} = \% \text{ of hydroxyapatite} \quad \text{(Eq. 3)}$$

2.3.4 - Cytotoxicity

Cytotoxicity test was performed according to previous work (34), with adaptations from (35). In order to summarize, the glass-ceramic powders were pre-incubated in culture medium (DMEM low glucose, with 10% bovine serum and 1% penicillin), 2 $mg.mL^{-1}$, and placed in a cell incubator for 24 h (37°C, 5% CO_2). Then, the solutions were filtered, and the powders were incubated again in the culture medium for 48 h (37°, 5% CO_2). This process avoids the burst release of ions that could lead to an increase in pH, enabling proper conditions for cell culture studies with glasses and glass-ceramics materials (35). The solutions were filtered and diluted in different concentrations (from 100% to 3.125%).

Osteoblastic precursor line cells derived from Mus musculus (mouse) calvaria (MC3T3-E1, ATCC, Brazil) were plated on 96-well plates at a concentration of 10^3 cells/well, using regular culture medium, and maintained in a cell incubator for 24 hours. Then, the cell culture medium was replaced by the conditioned medium in different dilutions (100%, 50, 25, 12.5, 6.25 and 3.125 %v/v – the volume of conditioned medium dissolved in regular culture media), and the materials were incubated for 72 hours (37°C, 5% CO_2). The cell viability was measured using MTT reduction assay, following procedures described elsewhere (8,36).

3. RESULTS

Figure 1 shows the XRD and DLS results of the obtained GCFe glass-ceramic powders. Figure 1a shows the X-ray diffractograms of the studied powders, which are characterized by the presence of peaks related to the crystalline structure of hematite (α-Fe_2O_3, ICDD 1-072-

0469). These peaks, related to hematite, are more pronounced in those glass-ceramics containing a higher fraction of iron oxide in their nominal compositions. Quantitative results about crystallinity degree and crystallite size are shown in Table 2. As more iron oxide was added in the glass structure, there was an increase of hematite crystal size (from 26 to 31 nm) and hematite fraction (11% up to 28%) in the final glass-ceramic powders.

Particle size measurements of glass-ceramics are presented in Fig. 1b-d. In general, the glass-ceramic powders showed a monomodal distribution between 70 and 700 nm. The mean particle size varied from 359 nm to 729 nm (Table 2). Iron oxide content in the material composition seems to decrease particle size along with the sol-gel synthesis. These results suggest an influence of the iron content on the particle size, which could deserve further investigation in the future. In principle, acting on the size-composition relationship to tailor the particle dimensions shows promise for a fine and function-driven design of these materials.

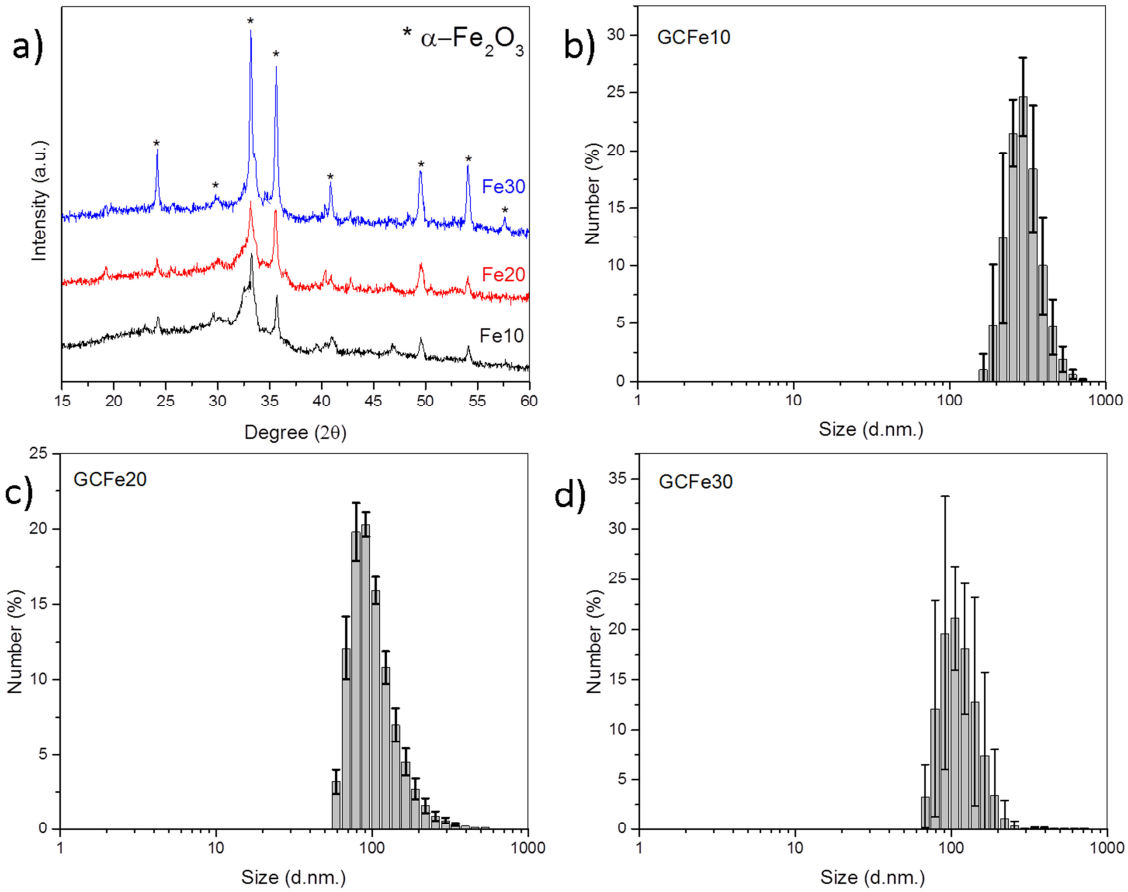

Figure 1. XRD and DLS results of the glass-ceramic powders: a) X-ray diffractograms ; b-d: Dynamic light scattering results of the CGFe10 (b), CGFe20 (c) and CGF30 (d) glass-ceramic powders. The * symbol in the XRD results denotes crystalline peaks related to hematite phase (α-Fe_2O_3, ICDD 1-072-0469)

Table 2. Quantitative results after XRD and DLS experiments: mean particle size, hematite nanocrystal size, and crystalline phase quantification.

Composition	Glass-ceramic particle size (nm)	Hematite nanocrystal size (nm)	Crystalline phase quantification (%)
GCFe10	729 ± 70	26	11
GCFe20	354 ± 89	27	23
GCFe30	484 ± 129	31	28

The magnetic measurements of the GCFe glass-ceramics were performed to characterize the magnetic behavior of the crystallized hematite phase (M-H curves), and also to verify the superparamagnetic behavior of such glass-ceramics (FC-ZFC curves). Fig. 2a shows the M-H curves at room temperature of the GCFe glass-ceramics, which present an intermediate behavior between superparamagnetic and weak ferrimagnetic. The GCFe10 and GCFe20 powders showed hysteresis, with relatively low residual magnetization (M_R) and coercive field (H_C) (Table 3). On the other hand, the GCFe30 powder shows no M_R and H_C, which is typical of superparamagnetic glass-ceramics (37,38). The maximum magnetization (M_{max}) at 60 kOe suggests that GCFe10 shows a lower magnetization compared to GCFe20 and GCFe30, which exhibited the same values of M_{max}.

Fig. 2b presents the FC-ZFC (M-T curves) of the GCFe glass-ceramics. The obtained results are typical of superparamagnetic materials, which exhibit a blocking temperature. Above the blocking temperature, the spins of the magnetic crystals can overcome an energy

barrier for magnetization reorientation, and they can therefore contribute to magnetization. However, the energy barrier for magnetization reorientation is dependent on the hematite crystal size.

Considering that these glass-ceramics have a distribution of hematite crystal size, we assume a distribution of energy barrier and a consequent distribution of blocking temperature. The maximum of the ZFC curve ($\delta M/\delta T = 0$) is considered as the mean blocking temperature (T_B). Therefore, the ZFC curves have an increase in magnetization as a function of temperature because spins have enough energy to overcome the energy barrier to align them with the applied magnetic field; in other words, it means that the particle temperature is above its blocking temperature (4,37). In contrast, in the FC curves, the particle magnetization is frozen under the external applied magnetic field. Thus, upon lowering the temperature, there is an increase in the magnetization, following a Curie's Law (4). At a given temperature, ZFC and FC curves meet one another. This point is known as irreversible temperature (T_{irr}) that is the temperature where the largest magnetic domain has its magnetization aligned with the applied magnetic field ($T > T_{irr}$). Therefore, the difference between T_B and T_{irr} gives an approximation of the energy barrier distribution due to magnetic anisotropy of the magnetic crystals dispersed in the glass matrix. The values of the blocking and irreversible temperature are reported in Table 3.

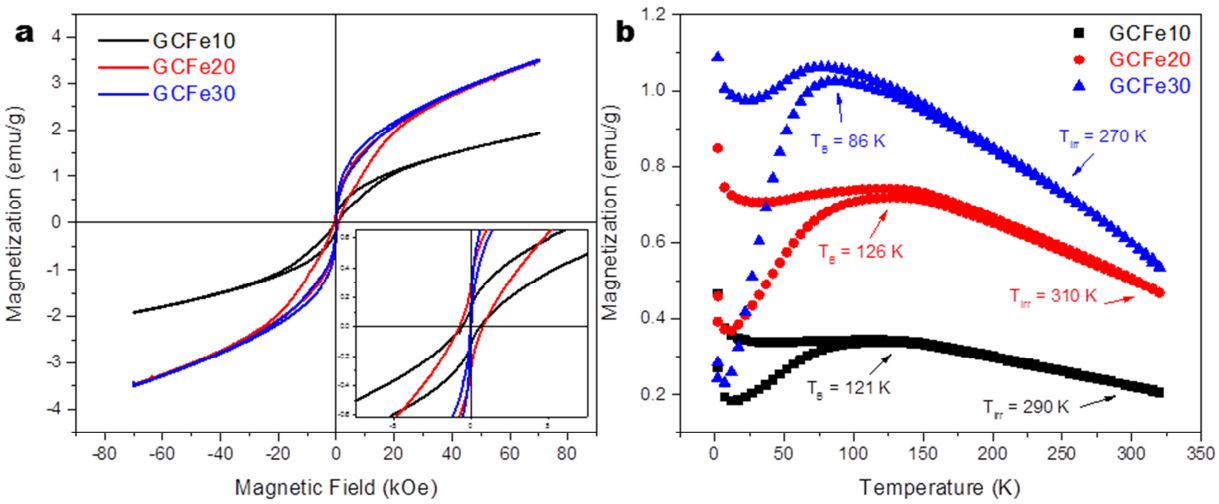

Figure 2. Magnetic characterization of GCFe glass-ceramics: a) room temperature magnetization as a function of the applied magnetic field (M-H curve); in detail the M-H curves near to M_R and H_C; b) temperature-dependent at 500 Oe FC-ZFC curves (field cooling, zero-field cooling) (M-T curves) showing blocking temperature (T_B) and irreversibility temperature (T_{irr}).

Table 3. Magnetic properties of GCFe glass-ceramics: maximum magnetization (M_{max}), coercive field (H_C), residual magnetization (M_R), blocking temperature (T_B), and irreversible temperature (T_{irr}).

	M_{max} (emu/g)	H_c (kOe)	M_R (emu/g)	T_B (K)	T_{irr} (K)
GCFe10	1.91	0.52	0.12	126	290
GCFe20	3.49	0.76	0.26	121	310
GCFe30	3.49	~0.0	~0.0	86	270

The calorimetric experiments (Figure 3) show that all three glass-ceramic compositions are capable of releasing heat when exposed to an alternating magnetic field. The temperature increases linearly over time up to 10 min from the beginning of the experiment. Then, the temperature increment becomes progressively less pronounced. As a whole, the experimental data follows a sigmoid-type trend that can be well approximated by a variety of mathematical functions. Least-squares fitting using a cubic polynomial model yields an excellent interpolation with $R^2 > 0.99$ for all the three datasets. Interestingly, an increased amount of iron in the composition does not seem to yield an increased ability of materials to develop heat, as revealed by the marked overlapping among the three curves.

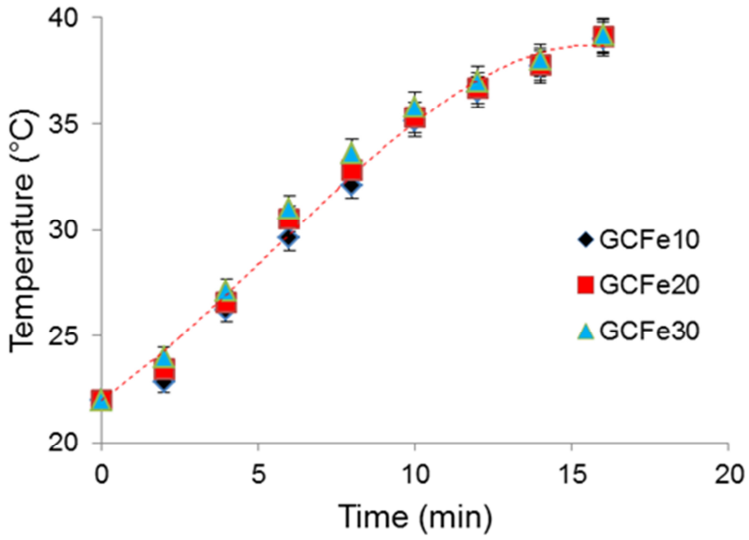

Figure 3. Calorimetric tests showing the capability of the GCFe glass-ceramics to develop heat over time. The red dashed sigmoidal curve has resulted from the fitting of the GCFe20 dataset with a cubic model.

Figures 4-6 show the results of the bioactivity test. The XRD results of the GCFe glass-ceramics before and after 1 and 7 days immersed in SBF solution are presented in Fig. 4. Overall, the observed peaks in the diffractograms correspond to the hematite phase, similar to the XRD results from Fig. 1a. Peaks related to a possible apatite phase were not apparently detected for any studied composition. However, the absence of such peaks in the XRD patterns does not necessarily mean that an apatite-like actually did not form, but could be due to (i) the low amount of this newly-formed phase (low rate of bioactive reactions) and (ii) the overlap with the hematite peaks (the major peak of hydroxyapatite is around 32°, very close to the major peak of α-Fe_2O_3).

SEM-EDS results of the GCFe glass-ceramics are presented in Figure 5. By analyzing the increase in color intensity with time of the compositional mapping by EDS, it is possible to qualitatively observe whether calcium and phosphorus were deposited on the glass-ceramic surface in order to form an apatite phase. All the glass-ceramics showed an increase in color intensity for calcium element (yellow) after 1 and 7 days immersed in the SBF solution, which however was not associated an increase in color intensity for phosphorus (green). This suggests that calcium and phosphorous did not precipitate at the same time on the glass-ceramic surface. This fact could also be supported by the XRD data, which revealed no apparent apatite phase deposition on the glass-ceramic surfaces for all compositions. Besides, an increase in color intensity of iron (purple) was observed in all the materials after immersion in the SBF solution, which may suggest exposure of the hematite nanocrystal with time.

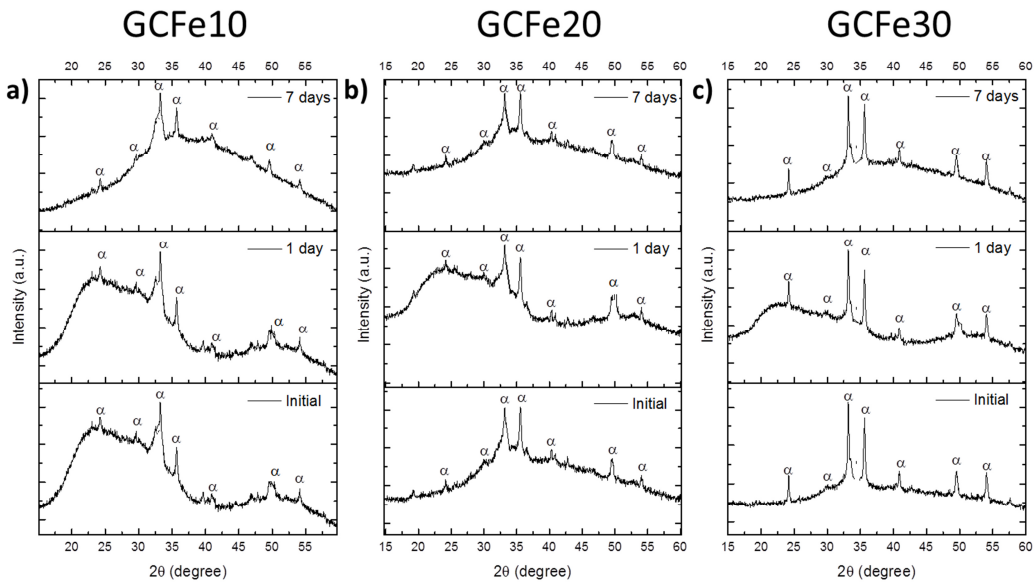

Figure 4. XRD results of the GCFe10 (a), GCFe20 (b) and GCFe30 (c) systems before and after immersion in SBF solution for 1 and 7 days. The α symbol assigns the hematite peaks (α-Fe_2O_3, ICDD 1-072-0469).

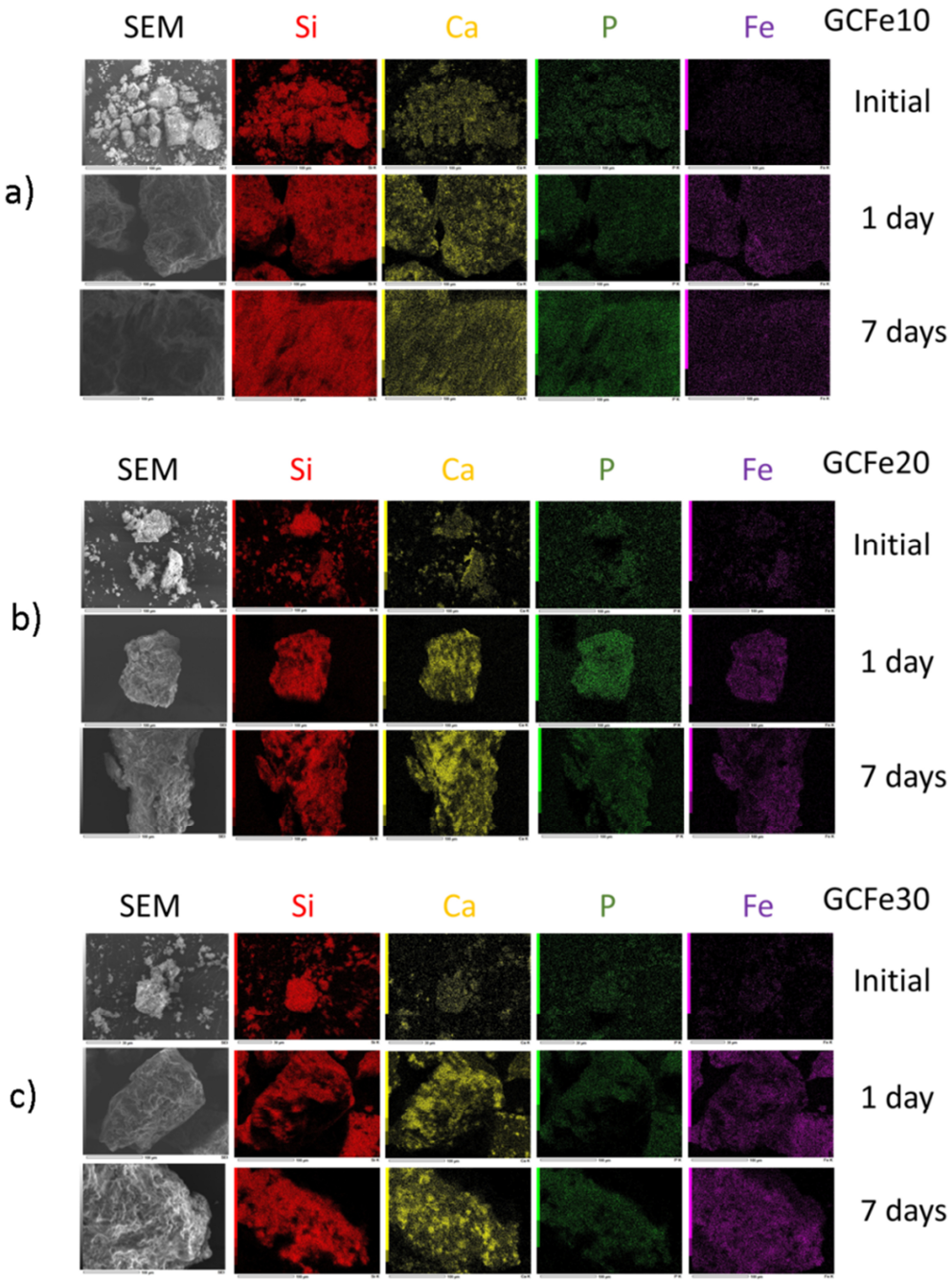

Figure 5. SEM images of the GCFe10 (a), GCFe20 (b) and GCFe30 (c) glass-ceramics before and after immersion in SBF solution for 1 and 7 days. EDS images show elemental analysis mapping of silicon (red), calcium (yellow), phosphorous (green), and iron (purple).

FTIR results from bioactivity tests are presented in Figure 6. All the studied systems showed the following functional groups: $P=O_{cryst}$ (585 and 605 cm^{-1}), $P=O_{glass}$ (585 cm^{-1}), structural SiO_2 (800 cm^{-1}), Q^0 (875 cm^{-1}), Si-OH (956 cm^{-1}), PO_3^{2-} (1030 cm^{-1}), Si-O- (1063 cm^{-1}), P=O (1100 cm^{-1}), Q^3 (1135 cm^{-1}) and Q^4 (1200 cm^{-1}) (39–41). Among these observed functional groups, structural SiO_2, Q^0, Si-OH, Si-O-, $Q^{3,}$ and Q^4 belongs to the glass-ceramic structure, while the functional groups PO_3^{2-} $P=O_{cryst}$, $P=O_{glass,}$ and P=O may either belong to the glass-ceramic structure or calcium phosphate deposited on the glass surface. Furthermore, the functional groups PO_3^{2-} and P=O can be found in amorphous or crystalline phosphate compounds, while the $P=O_{cryst}$ and $P=O_{glass}$ are specific of crystalline and amorphous phosphate phases, respectively. These two last-mentioned chemical bonds are interesting because they allow identifying whether the calcium phosphate deposited on the glass-ceramic surface is crystalline or not. It is worth mentioning that the detection of crystalline calcium phosphate is not always possible by XRD when thin and discontinuous layers of calcium phosphate are formed, and FTIR should be used as a complementary technique to characterize the bioactive behavior of glasses and glass-ceramics.

Figure 6d-f shows the region where crystalline and amorphous phosphate groups can be distinguishable. Before immersion in the SBF solution, there is no resolution to distinguish $P=O_{crys}$ and $P=O_{glass}$ bonds for all studied systems. After immersion in the SBF solution for 1 or 7 days, the intensity of these bonds increased, but they keep overlapped. Therefore, such phenomena suggest that calcium phosphate deposits could be either crystalline or amorphous.

Figure 7 shows the quantification of phosphate in GCFe glass-ceramics before (day 0) and after immersion in the SBF solution (days 1 and 7). The results evidenced an increase in

calcium phosphate phase deposited on the glass-ceramic surface as the glass-ceramics remained immersed in the SBF solution. This finding suggests that these glass-ceramics actually exhibit a bioactive behavior, which is characterized by the deposition of calcium phosphate on their surface. Furthermore, the in vitro bioactivity process is usually divided into five steps (please, see the reference (16) to read all the steps in detail), in which the two last ones refer to the precipitation of an amorphous calcium phosphate phase and crystallization of this phase into hydroxyapatite, respectively. Thereby, even though the calcium phosphate phase was not fully crystalline on GCFe glass-ceramics, its formation may indeed be associated to the two last steps involved in the bioactivity mechanism.

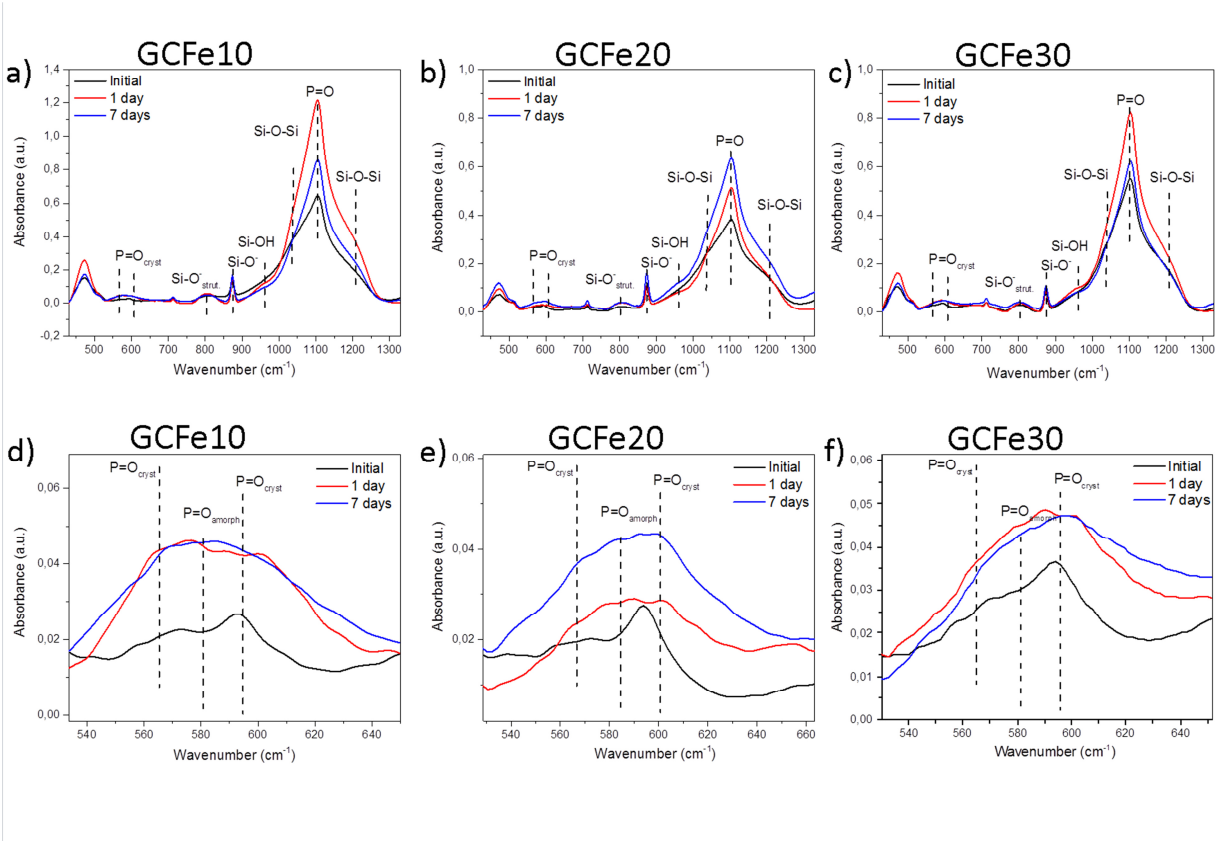

Figure 6. FTIR spectra of GCFe glass-ceramics before (in black) and after immersion in SBF solution for 1 (in red) and 7 days (in blue) for compositions: a) GCFe10; b) GCFe20; c) GCFe30. Detail of the phosphates bands between 520 and 660 cm^{-1} for compositions: d) GCFe10; e) GCFe20; f) GCFe30.

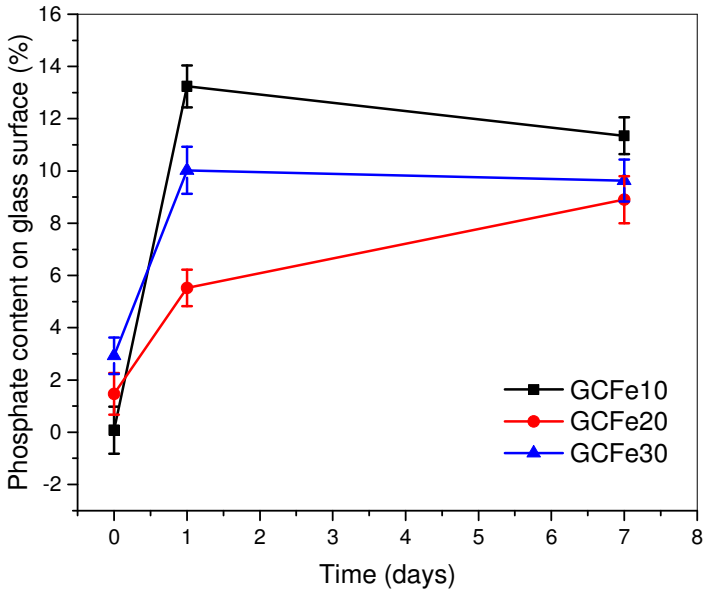

Figure 7. Phosphate quantification of GCFe glass-ceramics before and after immersion in the SBF solution. Data quantified from FTIR results presented in Figure 6.

Figures 8 and 9 present the cytotoxicity results regarding the cell morphological characterization and viability, respectively. Figure 8 shows the morphological characterization of MC3T3-E1 cells after conditioned medium at concentrations of 100, 25, and 3.125%. Some debris was noted for those cells treated with culture medium containing 100 % of conditioned (Fig. 8a, 8d, and 8g), which were more expressive in conditioned media from glass-ceramics containing a lower fraction of iron oxide. For those cells treated with more diluted conditioned

media, cell culture showed suitable confluency and less pronounced quantities of debris. The quantity of debris was also higher in those conditioned media derived from glass-ceramics containing a lower fraction of iron oxide.

In general, the cell viability after treatment with conditioned medium (Figure 9) is similar for all glass-ceramic compositions at the same concentration. An exception was observed in the conditioned media derived from the GCFe20 system at 25 and 12.5 %, which showed significantly lower viability compared to other systems.

A decrease in cell viability was observed in a more concentrated conditioned medium, suggesting a cytotoxic effect of the glass-ceramic systems on pre-osteoblastic cells. When the conditioned medium was diluted, the cell viability increased. For example, cell culture media containing from 3.125 to 12.5 % of conditioned medium showed cell viability higher than 70 %, which is suitable for biomedical applications.

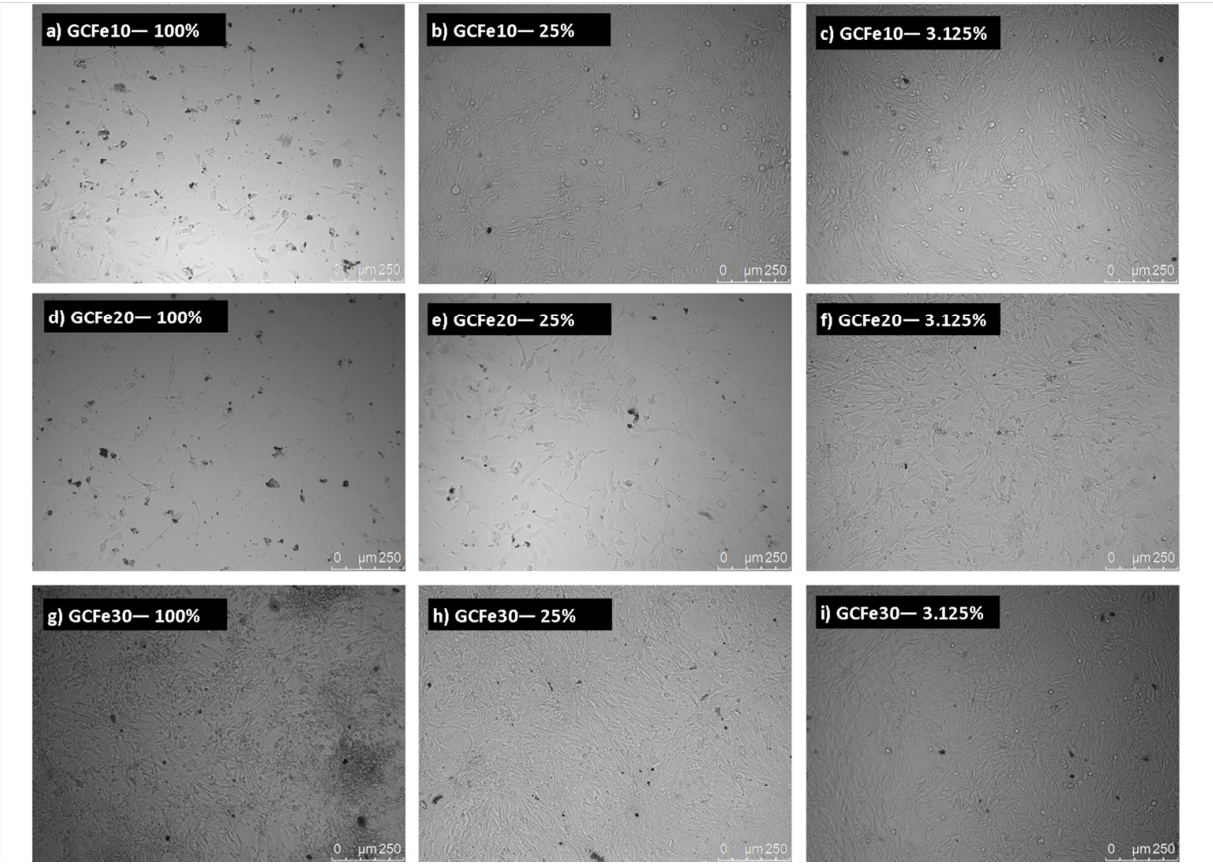

Figure 8. Morphological features of MC3T3 cells after GCFe systems incubation in conditioned medium at different concentrations. Left images:100%; Middle images: 25%; Right images: 3.125%. First line: GCFe10; second line: GCFe20; third line: GCFe30.

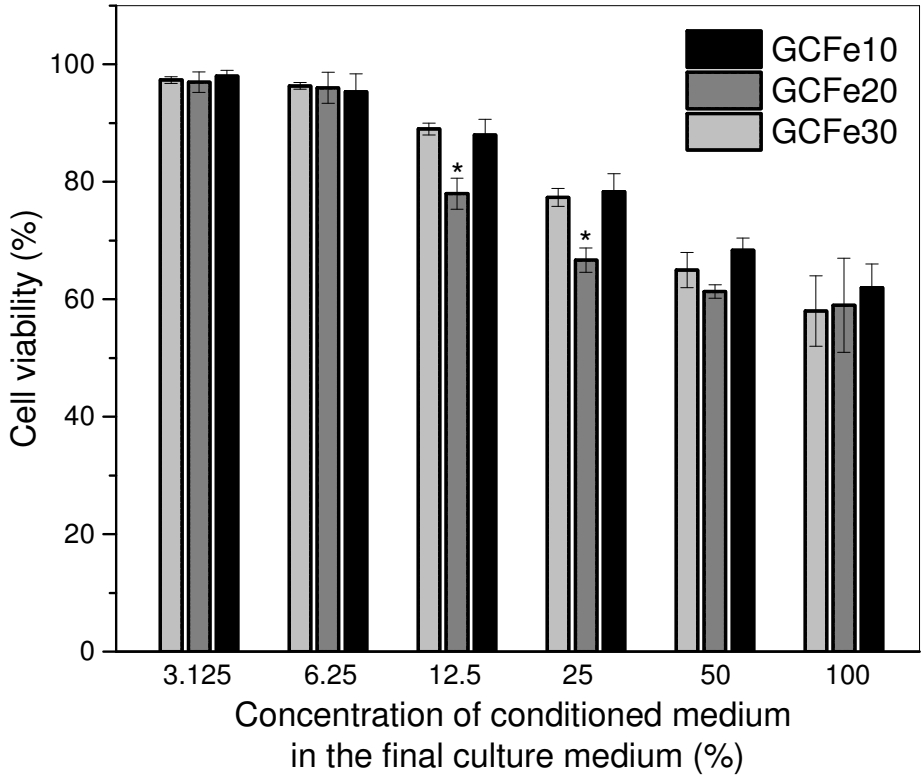

Figure 9. Cell viability from MTT assay of MC3T3-E1 cells in culture medium containing different fractions of GCFe glass-ceramics conditioned medium. * statistical significance of compositions in the same concentration, p-value < 0.05.

4. DISCUSSION

This work explored the potential of bioactive and superparamagnetic properties derived from new glass-ceramics containing hematite nanocrystal for applications in magnetic hyperthermia. To the best of the authors' knowledge, it is the very first time that the magnetic properties of nano-hematite are studied in bioactive glass-ceramics produced by sol-gel

method. Although hematite nanocrystals or nanoparticles have lower magnetization than maghemite or magnetite, hematite's superparamagnetic properties for hyperthermia applications have been underestimated in the field of biomaterials.

We proposed a one-pot sol-gel synthesis for the production of glass-ceramics containing hematite nanocrystals, and the initial XRD results (Figure 1) showed that it was possible to obtain such materials by the suggested methodology. The XRD results (Table 2) also evidenced that the iron oxide content influenced the fraction of hematite nanocrystals because those compositions containing a higher amount of iron oxide also showed a higher crystallinity index. However, the hematite crystal size was slightly influenced by the iron oxide content in the material composition. These results suggest that iron oxide content in the glass-ceramic composition influenced the crystal nucleation, but not necessarily the crystal growth. This is an interesting result because it means that crystal size is independent of iron content, which contributes to the obtainment of hematite nanocrystals with superparamagnetic properties regardless of the iron content in the glass-ceramic.

Moreover, the magnetic characterization suggested that the hematite crystals were in the nanoscale because of their superparamagnetic behavior, evidenced by the FC-ZFC curves. Superparamagnetic hematite nanocrystals are characterized by a blocking temperature and an irreversible temperature, i.e., the temperatures at which the mean-sized and bigger hematite crystals become superparamagnetic, respectively. The GCFe10 and GCFe20 glass-ceramics showed the highest values of irreversible temperature, 290 and 310 K, respectively, which are near to the temperature at which the M-H curves were collected (300 K). Given that superparamagnetic materials are supposed to only show H_c higher than zero at a temperature

above the blocking temperature (2), the hysteresis loops observed in the M-H curves of GCFe10 and GCFe20 glass-ceramics (Figure 2a) may be related to their high values of T_{irr}. Consequently, the GCFe30 glass-ceramic showed nearly-zero H_c due to its lower values of T_{irr} (270 K).

Additionally, the GCFe30 and GCFe20 glass-ceramic systems showed the same saturation magnetization, suggesting that both samples had a similar concentration of superparamagnetic crystals. Indeed, the crystallinity index obtained from the XRD results showed that both compositions had a similar amount of hematite (23 and 28 %, respectively). By having almost the same amount of hematite nanocrystals, the capability to develop heat of the glass-ceramic samples, if exposed to an alternating magnetic field, is almost insensitive to the amount of iron in the material composition, as shown by the overlapping of the temperature-time curves in Figure 8.

Furthermore, the magnetic characterization performed in our work suggests that the glass-ceramics produced by our sol-gel method are potentially suitable materials for applications in hyperthermia. If compared with other sol-gel-derived magnetic bioactive glass-ceramics, these GCFe glass-ceramics have magnetization properties close to the best results found so far; specifically, the values of M_{sat} (1.91-3.49 emu/g) are in the range typically reported in the literature (1-4 emu/g) (17, 35). Moreover, our materials have magnetic properties derived from superparamagnetic hematite, while most of the works from the literature report these properties as derived from maghemite or magnetite that are inherently ferrimagnetic. Interestingly, the saturation magnetization of our GCFe glass-ceramics is up to 100 times higher compared to the range reported for hematite nanoparticles covered with silicon dioxide in a core-shell structure (0.02-0.05 emu/g (42)), which is a system quite similar to

that proposed in this work. Therefore, our proposed hematite-containing glass-ceramics show great promise for hyperthermia applications being apparently more efficient, from a magnetic viewpoint, than the analogous options developed so far.

In addition, the calorimetric results reported here showed that the ability of these glass-ceramics to produce heat was not affected by the amount of crystalline phase present in their structure. These results support the potential suitability of the developed material for cancer treatment via a hyperthermic effect. Magnetic induction of hyperthermia is based on using magnetic materials to generate heat in the diseased site under the application of an external magnetic field (3,43). In clinical applications, heat is typically generated by applying an alternating magnetic field to the magnetic materials that were previously implanted or injected into the tumor site in order to increase and maintain the local temperature slightly above 40 °C, which our GCFe glass-ceramics were shown able to do (Figure 5). Malignant cells are then selectively killed as heat is slowly dissipated in cancerous tissues due to the lack of a well-organized vascular network (44).

Regarding the bioactivity test, XRD and SEM results suggest that calcium phosphate deposition in vitro was affected by the presence of hematite nanocrystals in the glass-ceramics. Although the apatite-forming ability was not totally suppressed, these GCFe glass-ceramics were found to be less bioactive as compared to the parent Fe-free 58S glass [ref]. Additionally, the FTIR results brought interesting information. Despite the $P{=}O_{cryst}$ and $P{=}O_{glass}$ chemical bonds were not well defined in the FTIR spectra, the quantification of phosphate groups showed that all the glass-ceramics had more phosphate groups after immersion in SBF solution. Such fact implies that calcium phosphate was actually deposited on the glass surface, but the

nature of this calcium phosphate (amorphous or crystalline) is not defined. Perhaps, if the samples would remain in SBF solution for a longer period, some well-defined crystalline phosphate groups could be seen in the FTIR spectra. Thus, the crystallization of this calcium phosphate into hydroxyapatite might not be excluded in the long-term.

Finally, the cytotoxicity results performed with MC3T3-E1 pre-osteoblastic cells evidenced that the CGFe glass-ceramics showed moderate cytotoxic effect at concentrated conditioned medium, which may be related to two factors: 1) the origin of the cell linage; 2) the iron oxide content in these materials. In the first case, pre-osteoblastic cells derived from mouse are more sensitive to the ionic dissolution products of bioactive glass-ceramics, which leads to an increase in apoptosis when compared to cell cultures using human lineages (45). Thereby, the cytotoxicity results found in this study can be even better if conducted in human pre-osteoblastic linages from primary culture.

Regarding the iron content, it is reported in the literature that magnetic bioactive glass-ceramics may show cytotoxicity around 60 % using the conditioned medium at 100 % (18,46), which agrees with the results reported here. The difficulty in establishing a straightforward comparison between our results and other results from the literature is related to different cell lineages and cell culture protocols. However, it is assumed that glass-ceramics containing iron oxide phases can induce the formation of reactive oxygen species (ROS) in the culture medium, which causes oxidative stress in cells, and thus decreases cell viability (18,46). The formation of ROS is due to the high reactivity of nano-sized iron oxide crystals (47). Furthermore, in the literature [ref], the effect of ROS is less pronounced after seven days of cell incubation in

conditioned medium or direct contact with cells. Thus, if our cytotoxicity test was performed in longer periods, we could observe improved viability results.

Besides, if these glass-ceramics are used in composite materials (like polymeric scaffolds or injectable hydrogels), diminished cytotoxicity is expected, and it could enable improved biological properties in terms of biocompatibility (12,48,49). Such decrease in cytotoxicity can occur because glasses and glass-ceramics dissolves under slower kinetics when present in composite materials, which mimics the cytotoxicity results of those diluted conditioned medium from Figure 9.

5. CONCLUSIONS

In this work, a new sol-gel route was developed in order to produce magnetic bioactive glass-ceramics for potential applications in cancer treatment by magnetic hyperthermia. Bioactive glasses containing iron oxide were thermally treated to promote the nucleation of hematite nanocrystals with superparamagnetic properties, which were studied for the first time in bioactive sol-gel glass-ceramics. It was found that crystallization does not become more efficient with the iron oxide content, indicating that there is a limitation in hematite crystals nucleation and growth. Such behavior also restricts the superparamagnetic properties, which are dependent on the crystalline fraction. The hyperthermia results suggested that our superparamagnetic glass-ceramic systems can develop heat if exposed to an alternating magnetic field. Furthermore, the GCFe glass-ceramics promoted the deposition of calcium phosphate during immersion in SBF solution, which is a proof of bioactivity, and showed

acceptable cytotoxicity levels. The overall results suggest that our glass-ceramics containing superparamagnetic hematite are promising materials for bone cancer treatment by hyperthermia.

6. ACKNOWLEDGMENT

This study acknowledge the facility support provided by UFABC, specially Central Experimental Multiusuário of the Universidade Federal do ABC (CEM-UFABC), and Department of Applied Science and Technology of Politecnico di Torino. Also, the authors appreciate the financial support provided by Fundação de Amparo a Pesquisa do Estado de São Paulo (FAPESP) and Conselho Nacional de Pesquisa e Desenvolvimento Científico (CNPq).

7. REFERENCES

1. Jolivet J-P, Chanéac C, Tronc E. Iron oxide chemistry. From molecular clusters to extended solid networks. Chem Commun [Internet]. 2004;(5):477–83. Available from: http://xlink.rsc.org/?DOI=B304532N

2. Fougt M, Koch B, Bødker F, Hansen MF, Koch CB. Magnetic properties of hematite nanoparticles. Phys Rev B. 2000;61(10):6826–38.

3. Périgo EA, Hemery G, Sandre O, Ortega D, Garaio E, Plazaola F, et al. Fundamentals and advances in magnetic hyperthermia. Appl Phys Rev. 2015;2(4).

4. Bihlmayer G. Handbook of Magnetism. 2nd ed. Kronmuller H, Parkin S, editors. Jonh Wiley &

Sons; 2007.

5. Sohail A, Ahmad Z, Bég OA, Arshad S, Sherin L. A review on hyperthermia via nanoparticle-mediated therapy. Bull Cancer [Internet]. 2017;104(5):452–61. Available from: http://dx.doi.org/10.1016/j.bulcan.2017.02.003

6. Borges R, Da Silva AC, Marchi J. Evaluation of the bioactivity behavior of a 48 wt %SiO<inf>2</inf> bioglass through experiments in simulated body fluid. Vols. 727–728, Materials Science Forum. 2012.

7. Hench LL. The story of Bioglass. J Mater Sci Mater Med. 2006;17:967–78.

8. Lopez TCC, Diniz IMA, Ferreira LS, Marchi J, Borges R, de Cara SPHM, et al. Bioactive glass plus laser phototherapy as promise candidates for dentine hypersensitivity treatment. J Biomed Mater Res - Part B Appl Biomater. 2017;105(1).

9. Elmadjian T, Lopez TCC, Borges R, Marchi J, Marques MM, Marques MM. Proposta de tratamento para hipersensibilidade dentinária à base de biovidro em diferentes veículos. Estudo morfológico in vitro. Clin Lab Res Dent [Internet]. 2015;21(1):19. Available from: http://www.revistas.usp.br/clrd/article/view/83957

10. Cacciotti I, Lombardi M, Bianco A, et al. Sol-gel derived 45S5 bioglass: synthesis, microstructural evolution and thermal behavior. J Mater Sci Mater Med. 2012;23:1849–66.

11. Shankhwar N, Srinivasan A. Evaluation of sol-gel based magnetic 45S5 bioglass and bioglass-ceramics containing iron oxide. Mater Sci Eng C [Internet]. 2016;62:190–6. Available from: http://dx.doi.org/10.1016/j.msec.2016.01.054

12. Aspasio RD, Borges R, Marchi J. Biocompatible Glasses for Cancer Treatment. In: Marchi J, editor. Biocompatible glasses: from bone regeenration to cancer treatment [Internet]. 1st ed.

Switzerland: Springer International; 2016. p. 249–65. Available from: http://link.springer.com/10.1007/978-3-319-44249-5

13. Ohura K, Ikenaga M, Nakamura T, Yamamuro T. A Heat-Generating Bioactive Glass-Ceramic for Hyperthermia. J Appl Biomater. 1991;2:153–9.

14. Ebisawa Y, Sugimoto Y, Hayashi T, Kokubo T, Ohura K, Yamamuro T. Crystallization of (FeO , Fe2O3) -CaO-SiO2 Glasses and Magnetic Properties of Their Crystallized Products. Nippon Seramikkusu Kyokai Gakujutsu Ronbunshi. 1991;99(1):7–13.

15. Velasco M V, Souza MT, Crovace MC, Oliveira AJA De, Zanotto ED. Bioactive magnetic glass-ceramics for cancer treatment. Biomed Glas. 2019;5:148–77.

16. Kokubo T, Takadama H. How useful is SBF in predicting in vivo bone bioactivity? Biomaterials. 2006;27(15):2907–15.

17. Borges R, Marchi J. Sol-Gel Synthesis of Bioglasses: A Growth Kinetics Study by Dynamic Light Scattering. Adv Sci Technol [Internet]. 2016;102(November):18–23. Available from: http://www.scientific.net/AST.102.18

18. Concepcio M, Sa J, Guinoa EZDE, Ruiz-herna E, Arcos D. In Vitro Positive Biocompatibility Evaluation of Glass – Glass Treatment of Bone Tumors. Tissue Eng Part A. 2008;14(5):617–27.

19. Arcos D, Real RP. Biphasic materials for bone grafting and hyperthermia treatment of cancer. J Biomed Mater Res A. 2003;65(1):71–8.

20. Serrano MC, Arcos D. Glass – glass ceramic thermoseeds for hyperthermic treatment of bone tumors. J Biomed Mater Res A. 2006;79(3):533–43.

21. Baeza A, Arcos D, Vallet-Regí M. Thermoseeds for interstitial magnetic hyperthermia : from

bioceramics to nanoparticles. J Phys Condens Matter. 2013;25:484003–14.

22. Li X, Wang X, Hua Z, Shi J. One-pot synthesis of magnetic and mesoporous bioactive glass composites and their sustained drug release property. Acta Mater. 2008;56:3260–5.

23. Wu C, Fan W, Zhu Y, Gelinsky M, Chang J, Cuniberti G, et al. Multifunctional magnetic mesoporous bioactive glass scaffolds with a hierarchical pore structure. Acta Biomater [Internet]. 2011;7(10):3563–72. Available from: http://dx.doi.org/10.1016/j.actbio.2011.06.028

24. Singh RK, Srinivasan A, Kothiyal GP. Evaluation of CaO –SiO2 – P2O5 – Na2O – Fe2O3 bioglass-ceramics for hyperthermia application. J Mater Sci Mater Med. 2009;20:147–51.

25. Singh RK, Srinivasan A. Magnetic properties of bioactive glass-ceramics containing nanocrystalline zinc ferrite. J Magn Magn Mater [Internet]. 2011;323(3–4):330–3. Available from: http://dx.doi.org/10.1016/j.jmmm.2010.09.029

26. Baino F, Fiume E, Miola M, Leone F, Onida B, Verné. E. Fe-doped bioactive glass-derived scaffolds produced by sol-gel foaming. Mater Lett. 2019;235:207–11.

27. Xia W, Chang J. Preparation and characterization of nano-bioactive-glasses (NBG) by a quick alkali-mediated sol-gel method. Mater Lett. 2007;61(14–15):3251–3.

28. Patterson AL. The Scherrer formula for X-ray particle size determination. Phys Rev. 1939;56:978–82.

29. Black DB, Lowering EG. Estimation of the degree of crystallinity in digoxin by X ray and Infrared methods. J Pharm Pharmacol. 1977;29:684–7.

30. Shah B, Kakumanu VK, Bansal AK. Analytical techniques for quantification of amorphous/crystalline phases in pharmaceutical solids. J Pharm Sci. 2006;95(8):1641–65.

31. Bruno M, Miola M, Bretcanu O, Vitale-Brovarone C, Gerbaldo R, Laviano F, et al. Composite bone cements loaded with a bioactive and ferrimagnetic glass-ceramic. Part I: Morphological, mechanical and calorimetric characterization. J Biomater Appl. 2014;29:254–267.

32. Maçon ALB, Kim T., Valliant EM, Goetschius K, Brow RK, Day DE, et al. A unified in vitro evaluation for apatite-forming ability of bioactive glasses and their variants . J Mater Sci Mater Med. 2015;25(2):115.

33. Yu Y, Bacsik Z, Eden M. Contrasting In Vitro Apatite Growth from Bioactive Glass Surfaces with that of Spontaneous Precipitation. Materials (Basel). 2018;3:20–2.

34. Zambanini T, Borges R, Faria PC, Delpino GP, Pereira IS, Marques MM, et al. Dissolution, bioactivity behavior, and cytotoxicity of rare earth-containing bioactive glasses (RE = Gd, Yb). Int J Appl Ceram Technol [Internet]. 2019 Jul 15;16(5):2028–39. Available from: https://onlinelibrary.wiley.com/doi/abs/10.1111/ijac.13317

35. Ciraldo FE, Boccardi E, Melli V, Westhauser F, Boccaccini AR. Tackling bioactive glass excessive in vitro bioreactivity: Preconditioning approaches for cell culture tests. Acta Biomater. 2018;75:3–10.

36. Marchi J, Ribeiro C, Bressiani AH de A, Marques MM. Cell response of calcium phosphate based ceramics, a bone substitute material. Mater Res [Internet]. 2013;16(4):703–12. Available from: http://www.scielo.br/scielo.php?script=sci_arttext&pid=S1516-14392013000400003&lng=en&tlng=en

37. Mikhaylova M, Kim DK, Bobrysheva N, Osmolowsky M, Semenov V, Tsakalakos T, et al. Superparamagnetism of Magnetite Nanoparticles : Dependence on Surface Modification. Langmuir. 2004;(17):2472–7.

38. Mamiya H, Ohnuma M, Nakatani I, Furubayashim T. Extraction of blocking temperature distribution from zero-field-cooled and field-cooled magnetization curves. IEEE Trans Magn. 2005;41(10):3394–6.

39. Macdonald SA, Schardt CR, Masiello DJ, Simmons JH. Dispersion analysis of FTIR refl ection measurements in silicate glasses. J Non Cryst Solids. 2000;275:72–82.

40. Serra J, González P, Liste S, Chiussi S, León B, Pérez-Amor M, et al. Influence of the non-bridging oxygen groups on the bioactivity of silicate glasses. J Mater Sci Mater Med. 2002;13(12):1221–5.

41. Aguiar H, Serra J, González P, León B. Structural study of sol-gel silicate glasses by IR and Raman spectroscopies. J Non Cryst Solids [Internet]. 2009;355(8):475–80. Available from: http://dx.doi.org/10.1016/j.jnoncrysol.2009.01.010

42. Deka S, Singh RK, Kannan S. In-situ synthesis , structural , magnetic and in vitro analysis of α - Fe2O3 – SiO2 binary oxides for applications in hyperthermia. Ceram Int [Internet]. 2015;41(10):13164–70. Available from: http://dx.doi.org/10.1016/j.ceramint.2015.07.091

43. Hergt R, Andra W, D'Ambly CG, Hilger I, Kaiser WA, Richter U, et al. Physical limits of hyperthermia using magnetic fine particles. IEEE Trans Magn. 1998;34:3745–54.

44. Idrees M, Jebakumar A. A review on potential benefits of hyperthermia in the treatment of cancer. Acta Biomed Sci. 2014;1:98–104.

45. Bielby RC, Christodoulou IS, Pryce RS, Radford WJ., Hench LL, Polak JM. Time- and Concentration-Dependent Effects of Dissolution Products of 58S Sol–Gel Bioactive Glass on Proliferation and Differentiation of Murine and Human Osteoblasts. Tissue Eng. 2004;10(7):1018–26.

46. Bretcanu O, Miola M, Bianchi CL, Marangi I, Carbone R, Corazzari I, et al. In vitro biocompatibility of a ferrimagnetic glass-ceramic for hyperthermia application. Mater Sci Eng C [Internet].

2017;73:778–87. Available from: http://dx.doi.org/10.1016/j.msec.2016.12.105

47. Swindle AL, Madden ASE, Cozzarelli IM, Benamara M. Size-Dependent Reactivity of Magnetite Nanoparticles: A Field- Laboratory Comparison. Environ Sci Technol. 2014;48(19):11413–20.

48. Zambanini T, Borges R, Marchi J. Bioactive glass/polymer composites for drug delivery. In: Gurbinder K, editor. Clinical Applications of Biomaterials: State-of-the-Art Progress, Trends, and Novel Approaches. 1st ed. Cham: Springer International Publishing; 2017.

49. Borges R, Kai KC, Marchi J. Biocompatible Glasses for controlled release technology. In: Marchi J, editor. Biocompatible glasses: from bone regeenration to cancer treatment [Internet]. 1st ed. Switzerland: Springer International; 2016. p. 285–315. Available from: http://link.springer.com/10.1007/978-3-319-44249-5